Dynamic Systems and Applications 32 (2023) 333-349

FINITE ELEMENT STUDY OF TRANSIENT MHD STOKES EQUATIONS AND MODELLING A DOUBLY DRIVEN CAVITY FLOW

ANIL RATHI, DIPAK KUMAR SAHOO, B.V.RATHISH KUMAR, MANISHA CHOWDHURY, AND SANGITA DEY

Department of Mathematics and Statistics, Indian Institute of Technology
Kanpur, India.

ABSTRACT. In this study, we derive a Galerkin finite element scheme for approximating the evolutionary Stokes Equations under magnetic effects which are governing a flow dynamics in a doubly driven cavity. The stable finite element numerical scheme is applied to trace the physics associated with the complex flow dynamics under the different MHD forces. The flow pattern is traced for different Hartmann and Reynolds Numbers and the obtained results are discussed in detail.

AMS (MOS) Subject Classification. 76D07, 65K15, 65M60.

Key Words and Phrases. Stokes MHD, Inclination angle, Reynolds number, Hartmann number.

1. INTRODUCTION

An essential fluid mechanical system, the lid-driven cavity serves as a standard for evaluating numerical approaches and for researching the fundamentals of incompressible flows in confined volumes that are propelled by the tangential motion of walls. It is well-known how important lid-driven cavity issues are for academic study. Besides the fundamental interest, the study of the lid-driven cavity has much practical importance such as short-dwell coating [1], transport processes in lakes can be studied by heating the side wall of cavity [2] and drug-reducing rib-lets [3-4]. In single lid-driven rectangular domains with various aspect ratios, researchers have been examining Newtonian [5-8] and non-Newtonian [9-11] fluid flow mechanics. In order to find solutions for higher Reynolds numbers and mesh refinements, Ghia et al. [12] examined the use of the multi-grid approach in the solution of the Navier-Stokes equation.

The square cavity powered by a double lid plays an important part in regulating the flow phenomenon. It is also useful in the mechanical and design fields. The double lid-driven cavity problem has attracted a lot of interest from scientists and

Received March 2, 2023 ISSN 1056-2176(Print); ISSN 2693-5295 (online)

https://doi.org/10.46719/dsa2023.32.18
www.dynamicpublishers.org Special Issue - ICNAAO 2022-IIT.

researchers in recent years because of its straightforward geometrical settings with all fluid mechanical applications, including cooling of electronic devices, drying tools, covering, softening processes, and so forth. Kuhlmann et al. [13] have extended the study of the Newtonian fluid flow problem in two-sided lid-driven rectangular domains for the first time in the literature. The authors have numerically and experimentally demonstrated the appearance of non-unique solutions in a non-square domain with two parallel walls moving at the same speeds but in the opposite direction from one another. Albensoeder et al. [14] have described several phases of Newtonian fluid flow solutions with symmetric and asymmetric main vortices in a rectangular domain. Blohm and Kuhlmann [15] looked at cellular instability in more detail. Later, using a variety of numerical techniques, Perumal and Dass [16-18], K:-T: Chen [19], Arun and Satheesh [20], and Caduo et al. [21] studied these characteristics for the Newtonian fluid flowing in two-sided lid-driven rectangular cavity issues. The time-dependent property of the Newtonian fluid flow solutions in rectangular domains driven by a two-sided lid has been studied by Hammami et al. [22].

Another active area of today's engineering applications is called magnetohydrodynamics (MHD), which deals with the interaction of magnetic fields with electrically conducting fluids. The literature has a strong foundation for MHD-based research, and the chemical, biological, medical, Bubble levitation, MHD pipe flows, and other applications are examples of MHD pipe flows [23-26]. S. Ganesh and S. Krishnambal [27] studied the Stokes Flow of a Viscous Fluid in an Unsteady Magnetohydrodynamic field Between Two Parallel Porous Plates. A mathematical analysis of laminar flow between two parallel porous plates with a linked magnetic field was published by Terrill and Shrestha [28]. Pirmohammadi and Ghassemi [29] investigated the impact of a magnetic field on convective heat transport. They discovered that the convection heat transfer decreases for a given inclination angle as the Hartmann number (Ha) rises. Transient MHD mixed convection flow in a lid-driven cavity with a heated wavy wall is discussed by [30].

In a single lid-driven cavity and backward-facing step channel, the MHD Stokes flow equations are solved in the presence of a uniform magnetic field with various directions studied by Merve Gürbüz and M. Tezer-Sezgin [31]. In the present work, we show all the numerical experiments for Doubly driven cavity flow, which has totally different physics from the case of single lid-driven cavity flow. The MHD Stokes flow in a Doubly driven cavity has not been studied in any published works.

In the present study, we have investigated the Newtonian Stokes Magnetohydrodynamic (Stokes MHD) fluid flow pattern in a doubly driven square cavity, where the top and bottom walls of the square domain rotate in a clockwise direction with unit magnitude and the other two walls have the no-slip condition (which means $u = (1, 0)$ and $u = (-1, 0)$ on top and bottom walls respectively and $u = (0, 0)$ on rest two walls

of the square domain). Here, we are varying Hartmann number Ha from 0 to 50 for fixing $Re = 1$. MHD (Magnetohydrodynamic) term depends on the inclination angle θ. Therefore, we have work for some different values of the inclination angle θ varies from 0 to $\frac{\pi}{2}$. This article reports various patterns of vortex formulation for a Newtonian fluid. In order to solve the fully discrete transient Stokes MHD fluid flow problem, we have used the Galerkin finite element approach with the Backward-Euler finite difference method in this instance, where the numerical scheme's accuracy, efficiency, and durability have all been carefully examined. Here, we have validated the performance of the method with the existing scheme in the literature. After the successful code-validation, we conducted the experiments in the domains for the different values of Hartmann number Ha ranges from 0 to 50 and the inclination angle θ ranges between 0 to $\frac{\pi}{2}$. Since the magnetic force depends on Hartmann's number and inclination angle. So, the main focus of this article is to see how the magnetic term affects the flow.

The organization of this article is as follows: Section 2 describes the mathematical problem and applies the Galerkin finite element method to governing equations followed by weak formulation. The numerical finding is displayed in the section 3, followed by validation tests. Conclusion on the numerical results in section 4.

2. PRELIMINARIES

2.1. **Governing Equations.** Let Ω be an open, bounded, polygonal domain in $\mathbb{R}^2$ with piece-wise smooth boundary $\partial\Omega$, for time interval $J := (0, T]$, The governing equations for an incompressible Stokes Magnetohydrodynamic fluid flow in $\Omega \times J$ are given by: find the velocity $\mathbf{u} = (u_1, u_2) : \Omega \times J \to \mathbb{R}^2$ and the pressure $p : \Omega \times J \to \mathbb{R}$ of the fluid such that

(2.1)
$$\frac{\partial u_1(x,t)}{\partial t} - \frac{1}{Re}\Delta u_1(x,t) + \frac{\partial p\,(x,t)}{\partial x_1} + \frac{Ha^2}{Re}(u_1(x,t)\sin^2\theta - u_2(x,t)\sin\theta\cos\theta) = f_1 \text{ in } \Omega\times J,$$

(2.2)
$$\frac{\partial u_2(x,t)}{\partial t} - \frac{1}{Re}\Delta u_2(x,t) + \frac{\partial p\,(x,t)}{\partial x_2} + \frac{Ha^2}{Re}(u_2(x,t)\cos^2\theta - u_1(x,t)\sin\theta\cos\theta) = f_2 \text{ in } \Omega\times J,$$

$$\nabla \cdot \mathbf{u} = 0 \text{ in } \Omega \times J, \tag{2.3}$$

$$\mathbf{u} = 0 \text{ on } \partial\Omega \times J, \tag{2.4}$$

$$\mathbf{u} = \mathbf{u}_0 \text{ at } t = 0, \tag{2.5}$$

where Re and Ha are Reynolds number and Hartmann number respectively.

2.2. **Weak Formulation.** Let $V = H_0^1(\Omega) := \{v_1 \in H^1(\Omega) : v_1 = 0 \ on \ \partial\Omega\}$, $Q = L_2(\Omega)/\mathbb{R} := \{q \in L_2(\Omega) : \int_\Omega q = 0\}$ and $X = V \times V \times Q$, now multiplying equation (1), (2) and (3) by test functions $v_1 \in V$, $v_2 \in V$ and $q \in Q$ respectively and integrating over Ω, we get variational formulation as:

(2.6)
$$(\frac{\partial u_1}{\partial t}, v_1) - \frac{1}{Re}(\Delta u_1, v_1) + (\frac{\partial p}{\partial x_1}, v_1) + \frac{Ha^2}{Re}[\sin^2\theta(u_1, v_1) - \sin\theta\cos\theta(u_2, v_1)] = (f_1, v_1) \ \forall v_1 \in V,$$

(2.7)
$$(\frac{\partial u_2}{\partial t}, v_2) - \frac{1}{Re}(\Delta u_2, v_2) + (\frac{\partial p}{\partial x_2}, v_2) + \frac{Ha^2}{Re}[\cos^2\theta(u_2, v_2) - \sin\theta\cos\theta(u_1, v_2)] = (f_2, v_2) \ \forall v_2 \in V,$$

$$(\nabla \cdot \mathbf{u}, q) = 0 \ \forall \ q \in Q. \tag{2.8}$$

Now using integration by parts and summing the equations (2.6), (2.7) and (2.8), we get

$$\left(\mathbf{M}\frac{\partial \mathbf{U}}{\partial t}, \mathbf{W}\right) + B(\mathbf{U}; \mathbf{W}) = L(\mathbf{W}) \ \forall \ \mathbf{W} \in X, \tag{2.9}$$

where $\mathbf{M} = diag(1, 1, 0)$, $\mathbf{U} = (u_1, u_2, p)$, $\mathbf{W} = (v_1, v_2, q)$,

$$(\mathbf{M}\frac{\partial \mathbf{U}}{\partial t}, \mathbf{W}) = (\frac{\partial u_1}{\partial t}, v_1) + (\frac{\partial u_2}{\partial t}, v_2) \ ,$$

$$B(\mathbf{U}; \mathbf{W}) = \frac{1}{Re}(\nabla \mathbf{u}, \nabla \mathbf{v}) - (p, \frac{\partial v_1}{\partial x_1}) - (p, \frac{\partial v_2}{\partial x_2}) + \frac{Ha^2}{Re}\sin^2\theta(u_1, v_1) + \frac{Ha^2}{Re}\cos^2\theta(u_2, v_2)$$
$$- \frac{Ha^2}{Re}\sin\theta\cos\theta(u_2, v_1) - \frac{Ha^2}{Re}\sin\theta\cos\theta(u_1, v_2) + (\nabla.\mathbf{u}, q),$$

$$L(\mathbf{W}) = (f_1, v_1) + (f_2, v_2),$$
$$(\nabla \mathbf{u}, \nabla \mathbf{v}) = (\nabla u_1, \nabla v_1) + (\nabla u_2, \nabla v_2),$$

where $\mathbf{u} = (u_1, u_2)$ and $\mathbf{v} = (v_1, v_2)$.

2.3. **Fully Discrete Formulation.** First, we use finite element space discretization to create the semi-discrete variational formulation. Let $T_h = \{K\}$ be the triangulation of $\Omega \subset \mathbb{R}^2$ such that T_h satisfies: there exist a positive constant C, independent of h such that

$$\frac{\gamma_K}{h_K} \geq C \ \forall K \in T_h.$$

where $h_K :=$ the diameter of K = longest side of triangle K and

$\gamma_K :=$ the diameter of the circle inscribed in K

$h := \max_{K \in T_h} h_K$

Due to this condition, the triangle $K \in T_h$ cannot be thinned arbitrarily, or equivalently, Triangles K cannot have arbitrarily small angles. Since $V = H_0^1(\Omega)$, let $V_h \subset V$ such that $V_h = \{v \in V : v|_K \in P_2(K)\}$, where $P_r(K)$ is the space of polynomials of degree $\leq r$ in K. Similarly, $Q_h \subset Q$ such that $Q_h = \{q \in Q : q|_K \in P_1(K)\}$ and $X_h = V_h \times V_h \times Q_h \subset X$. Here the subspaces V_h and Q_h are constructed by piecewise polynomials. A finite set of basis functions generates these subspaces. Therefore, V_h and Q_h are also finite-dimensional subspaces of V and Q as well X_h is a subspace of X. The standard Galerkin finite element formulation is given as: find $U_h = (\mathbf{u}_h, p_h) \in \mathbf{U}_h$ such that $\forall t \in J$

$$(\mathbf{M}\frac{\partial \mathbf{U}_h}{\partial t}, \mathbf{W}_h) + B(\mathbf{U}_h; \mathbf{W}_h) = L(\mathbf{W}_h)\ \forall \mathbf{V}_h \in X_h, \tag{2.10}$$

where $\mathbf{U}_h = (u_{1h}, u_{2h}, p_h)$ and $\mathbf{W}_h = (v_{1h}, v_{2h}, q_h)$.

Now for the fully discrete formulation, we discretized the time variable by *Backward Euler* scheme. So, time interval $[0, T]$ be partitioned into M sub-intervals, for some positive integer M. Let dt be the time step size defined as $dt = \frac{T}{M}$, an intermediate n^{th} time step, $t_n = ndt$ for $0 \leq n \leq M$. Let $v^n = v(x, t_n)$, So fully discrete form looks-like

$$(\mathbf{M}\frac{\mathbf{U}_h^{n+1} - \mathbf{U}_h^n}{dt}, \mathbf{W}_h) + B(\mathbf{U}_h^{n+1}; \mathbf{W}_h) = L(\mathbf{W}_h)\ \forall \mathbf{W}_h \in X_h, \tag{2.11}$$

where

$$(\mathbf{M}\frac{\mathbf{U}_h^{n+1} - \mathbf{U}_h^n}{dt}, \mathbf{W}_h) = (\frac{u_{1h}^{n+1} - u_{1h}^n}{dt}, v_{1h}) + (\frac{u_{2h}^{n+1} - u_{2h}^n}{dt}, v_{2h}),$$

$$B(\mathbf{U}_h^{n+1}; \mathbf{W}_h) = \frac{1}{Re}(\nabla \mathbf{u}_h^{n+1}, \nabla \mathbf{v}_h) - (p_h^{n+1}, \nabla . \mathbf{v}_h) + \frac{Ha^2}{Re}\sin^2\theta(u_{1h}^{n+1}, v_{1h}) + \frac{Ha^2}{Re}\cos^2\theta(u_{2h}^{n+1}, v_{2h})$$

$$-\frac{Ha^2}{Re}\sin\theta\cos\theta(u_{2h}^{n+1}, v_{1h}) - \frac{Ha^2}{Re}\sin\theta\cos\theta(u_{1h}^{n+1}, v_{2h}) + (\nabla \cdot \mathbf{u}_h^{n+1}, q_h),$$

$$L(\mathbf{W}_h) = (f_1, v_{1h}) + (f_2, v_{2h}).$$

From equation (2.11) we have

$$\frac{1}{dt}(\mathbf{M}\mathbf{U}_h^{n+1}, \mathbf{W}_h) + B(\mathbf{U}_h^{n+1}; \mathbf{W}_h) = L(W_h) + \frac{1}{dt}(\mathbf{M}\mathbf{U}_h^n, \mathbf{W}_h)\ \forall \mathbf{W}_h \in X_h, \tag{2.12}$$

$$A(\mathbf{U}_h^{n+1}, \mathbf{W}_h) = F(\mathbf{W}_h)\ \forall \mathbf{W}_h \in X_h, \tag{2.13}$$

where

$$A(\mathbf{U}_h^{n+1}, \mathbf{W}_h) = \frac{1}{dt}(\mathbf{M}\mathbf{U}_h^{n+1}, \mathbf{W}_h) + B(\mathbf{U}_h^{n+1}; \mathbf{W}_h)$$
$$= \frac{1}{dt}(\mathbf{M}\mathbf{U}_h^{n+1}, \mathbf{W}_h) + \frac{1}{Re}(\nabla \mathbf{u}_h^{n+1}, \nabla \mathbf{v}_h) - (p_h^{n+1}, \nabla.\mathbf{v}_h) + \frac{Ha^2}{Re}\sin^2\theta(u_{1h}^{n+1}, v_{1h})$$
$$+ \frac{Ha^2}{Re}\cos^2\theta(u_{2h}^{n+1}, v_{2h}) - \frac{Ha^2}{Re}\sin\theta\cos\theta\left[(u_{2h}^{n+1}, v_{1h}) + (u_{1h}^{n+1}, v_{2h})\right] + (\nabla.\mathbf{u}_h^{n+1}, q_h),$$
$$F(\mathbf{W}_h) = L(\mathbf{W}_h) + \frac{1}{dt}(\mathbf{M}\mathbf{U}_h^n, \mathbf{W}_h).$$

$A(.,.)$ is bilinear form on $X_h \times X_h$ and $F(.)$ is linear form on X_h as U_h^n is known.

Since, we are approximating the solution of equation (2.1)-(2.3) by using the Galerkin FE scheme, So, by equation (2.3) we have

$$\left(\nabla.\mathbf{u}_h^{n+1}, q_h\right) = 0 \ \forall \ q_h \in Q_h.$$

Now we can write

$$A(\mathbf{U}_h^{n+1}, \mathbf{W}_h) = a(\mathbf{u}_h^{n+1}, \mathbf{v}_h) + b(p_h, \mathbf{v}_h),$$

where,

$$a(\mathbf{u}_h^{n+1}, \mathbf{v}_h) = \frac{1}{dt}(\mathbf{u}_h^{n+1}, \mathbf{v}_h) + \frac{1}{Re}(\nabla \mathbf{v}_h, \nabla \mathbf{v}_h) + \frac{Ha^2}{Re}\sin^2\theta(v_{1h}, v_{1h}) + \frac{Ha^2}{Re}\cos^2\theta(v_{2h}, v_{2h})$$
$$- \frac{Ha^2}{Re}\sin\theta\cos\theta(u_{2h}^{n+1}, v_{1h}), -\frac{Ha^2}{Re}\sin\theta\cos\theta(u_{1h}^{n+1}, v_{2h})$$
$$b(p_h, \mathbf{v}_h) = -(p_h^{n+1}, \nabla \cdot \mathbf{v}_h).$$

Since, $\mathbf{U}_h = (u_{1h}, u_{2h}, p_h), \mathbf{W}_h = (v_{1h}, v_{2h}, q_h) \in X_h \subset X = H_0^1(\Omega) \times H_0^1(\Omega) \times L_2(\Omega)/\mathbb{R}$ by using Cauchy-Schwarz inequality we can easily get $a(.,.)$, $b(.,.)$ and $F(.)$ to be continuous functionals. Here $\|.\|$ is norm in $L_2(\Omega)$ space and $\|.\|_1$ is norm in $H^1(\Omega)$ space.

$$a(\mathbf{v}_h, \mathbf{v}_h) = \frac{1}{dt}(\mathbf{v}_h, \mathbf{v}_h) + \frac{1}{Re}(\nabla \mathbf{v}_h, \nabla \mathbf{v}_h) + \frac{Ha^2}{Re}\sin^2\theta(v_{1h}, v_{1h}) + \frac{Ha^2}{Re}\cos^2\theta(v_{2h}, v_{2h})$$
$$- \frac{Ha^2}{Re}\sin\theta\cos\theta(v_{2h}, v_{1h}) - \frac{Ha^2}{Re}\sin\theta\cos\theta(v_{1h}, v_{2h})$$
$$\geq \frac{1}{dt}\|\mathbf{v}_h\|^2 + \frac{1}{Re}\|\nabla \mathbf{v}_h\|^2 + \frac{Ha^2}{Re}[\sin^2\theta\|v_{1h}\|^2 + \cos^2\theta\|v_{2h}\|^2 - 2\sin\theta\cos\theta\|v_{1h}\|\|v_{2h}\|]$$
$$\geq \frac{1}{dt}\|\mathbf{v}_h\|^2 + \frac{1}{Re}\|\nabla \mathbf{v}_h\|^2 + \frac{Ha^2}{Re}\left(\|v_{1h}\|\sin\theta - \|v_{2h}\|\cos\theta\right)^2$$
$$\geq \frac{1}{dt}\|\mathbf{v}_h\|^2 + \frac{1}{Re}\|\nabla \mathbf{v}_h\|^2$$
$$\geq \min(\frac{1}{dt}, \frac{1}{Re})(\|\mathbf{v}_h\|^2 + \|\nabla \mathbf{v}_h\|^2)$$
$$= \min(\frac{1}{dt}, \frac{1}{Re})\|\mathbf{v}_h\|_1^2.$$

Therefore, $a(.,.)$ is a coercive bilinear form. For the particular chosen spaces V_h and Q_h The Babuška–Brezzi condition [32-33] is satisfied by [34] there exists a constant $\beta > 0$ such that

$$\sup_{\mathbf{v}_h \in V_h \times V_h, \mathbf{v}_h \neq 0} \frac{(q_h, \nabla.\mathbf{v}_h)}{\|\mathbf{v}_h\|_1} \geq \beta \|q_h\| \ \forall \ q_h \in Q_h.$$

Now if $A(\mathbf{U}_h, \mathbf{W}_h) = 0, \forall \mathbf{W}_h \in X_h$ then by taking particular value of $\mathbf{W}_h$ as $\mathbf{U}_h$,

$$\begin{aligned} & A(\mathbf{W}_h, \mathbf{W}_h) = 0 \\ & \implies \frac{1}{dt}\|\mathbf{u}_h\|^2 + \frac{1}{Re}\|\nabla \mathbf{u}_h\|^2 + \frac{Ha^2}{Re}(\|u_{1h}\| \sin\theta - \|u_{2h}\| \cos\theta)^2 = 0 \\ & \implies \mathbf{u}_h = \mathbf{0}. \end{aligned}$$

By using $\mathbf{u}_h = \mathbf{0}$ and $\nabla.\mathbf{v}_h \in Q_h$, we get $p_h = 0$. Therefore, $\{\mathbf{U}_h \in X_h : A(\mathbf{U}_h, \mathbf{W}_h) = 0, \forall \ \mathbf{W}_h \in X_h\} = 0$.

Now, using the theorem by Brezzi ([32],[35]) equation (2.13) has unique solution U_h^{n+1}.

3. MAIN RESULTS

This section offers some observations on the numerical results from the Stokes MHD problem numerical solution in a square domain with moving top and bottom walls, the square domain with top and bottom lids moving with velocities $(1, 0)$ and $(-1, 0)$, respectively.

3.1. Grid Validation.

To establish the optimal grid size, we first demonstrate the grid validation test. In a square domain with top and bottom walls moving horizontally to the right and left, respectively, with unit velocity and no-slip conditions on the right and left walls being set, we have carried out numerical tests for the incompressible Stokes MHD flow equations with $Re = 10$ and $Ha = 10$.

We selected mesh sizes **MS1:** 70×70**, MS2:** 80×80**, MS3:** 90×90, and **MS4:** 100×100 for the grid validation test. For grid sizes, MS1, MS2, MS3, and MS4, the horizontal and vertical velocity charts along $x_1 = 0.5$ and $x_2 = 0.5$ correspondingly show minimal changes. Therefore, 100×100 grids were selected as the best size for the entire study.

3.2. Code Validation.

Now, we have executed the numerical code validation test for the steady Stokes equation in a square domain. These experiments are carried out on a bounded square domain $\Omega = (0, 1) \times (0, 1)$

$$-\Delta u_1 + \frac{\partial p}{\partial x} = f_1 \text{ in } \Omega, \tag{3.1}$$

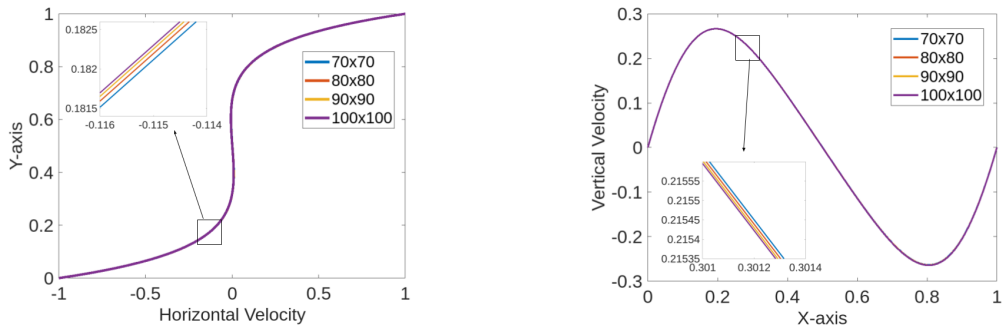

(A) Horizontal velocity along $x_1 = 0.5$ (B) Vertical velocity along $x_2 = 0.5$

FIGURE 1. Grid validation horizontal and vertical velocity

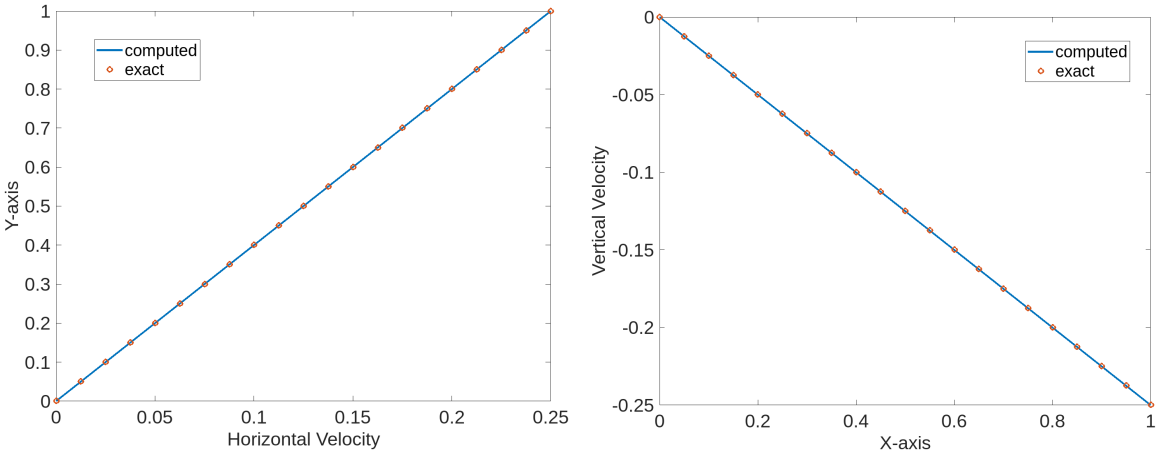

(A) Horizontal velocity along $x_1 = 0.5$ (B) Vertical velocity along $x_2 = 0.5$

FIGURE 2. Code validation horizontal and vertical velocity

$$-\Delta u_2 + \frac{\partial p}{\partial y} = f_2 \text{ in } \Omega, \tag{3.2}$$

$$\nabla \cdot \mathbf{u} = 0 \text{ in } \Omega. \tag{3.3}$$

The exact solution for this experiments are: $\mathbf{u} = (u_1, u_2) = (xy^2, -x^2y)$ and $p = 1 - x$ for compatible $f_1 = -1 - 2x$ and $f_2 = 2y$. In figure 2, we notice that horizontal velocity for $x_1 = 0.5$ (figure 2a) and vertical velocity for $x_2 = 0.5$ (figure 2b) has no significant change in computed solution and exact solution.

Here now we are also going to give a comparison with existing literature: Merve Gürbüz and M. Tezer-Sezgin [31]. In figure 3 we can see there is no significant change in the formation of vortices in the streamlines plot for Hartmann numbers $Ha = 1$, 30, and 80. Similarly, in figure 4, there is a comparison of horizontal and vertical velocity plots for Hartmann number $Ha = 1$, 30 and 80 with M. Tezer-Sezgin et. al [31] at $x_1 = 0.5$ and $x_2 = 0.5$ lines respectively. The velocities do not much vary in this instance either. So, We can state that the current scheme validates every single case

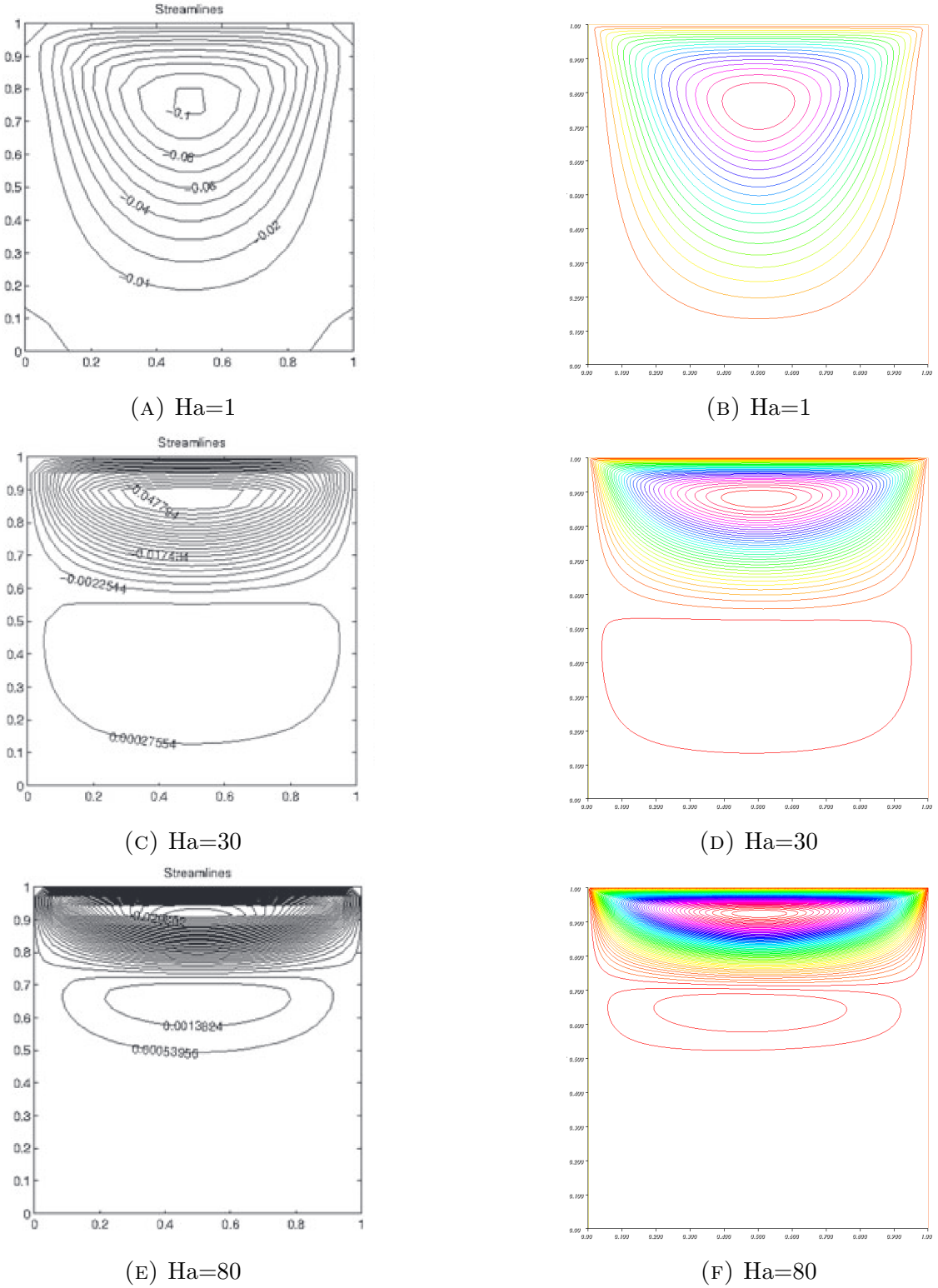

(A) Ha=1 (B) Ha=1

(C) Ha=30 (D) Ha=30

(E) Ha=80 (F) Ha=80

FIGURE 3. Comparison of Streamlines plots for $\theta = 0$ and $Ha = 1$, 30 and 80 in lid-driven cavity with M. Tezer-Sezgin's [31] scheme

of a single lid-driven cavity flow instance provided in the study of M. Tezer-Sezgin et. al [31].

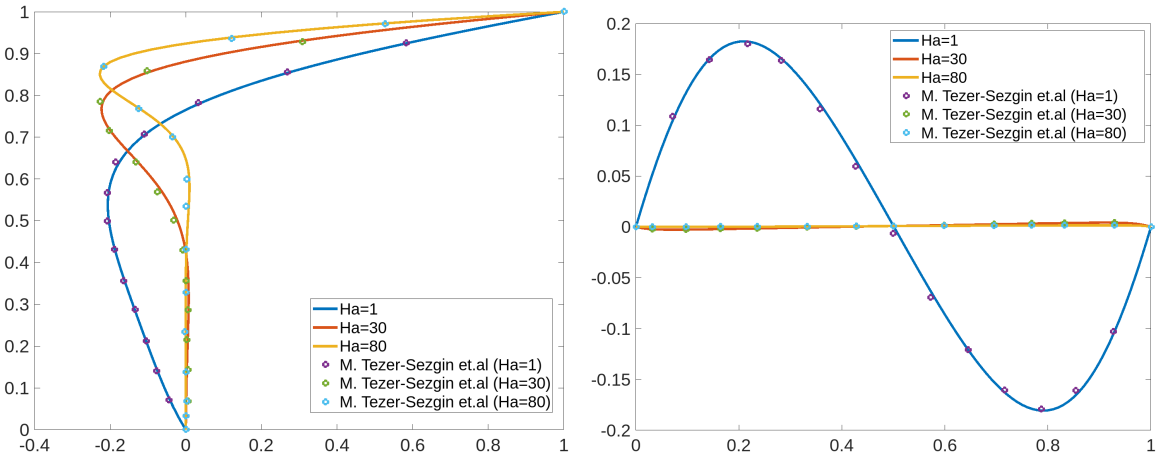

(A) Horizontal velocity along $x_1 = 0.5$ (B) Vertical velocity along $x_2 = 0.5$

FIGURE 4. Horizontal and vertical velocity comparison at $x_1 = 0.5$ and $x_2 = 0.5$ respectively with M. Tezer-Sezgin et. al [31] scheme

In the present work, we experiment with all the numerical results for Doubly driven cavity flow. Here we mainly focus on how the magnetic force and its direction affect the doubly driven cavity flow. In this work, the effect of magnetic force's direction in the doubly driven cavity is shown clearly by streamlines plots and velocity plots at mid-planes.

3.3. **Experiments.** Here, we have performed numerical experiments to examine the Stokes MHD fluid flow in the presence of moving top and bottom walls of the square domain in a clockwise direction (which implies the boundary conditions at these walls are $u = (1, 0)$ and $(-1, 0)$ respectively to the top and bottom walls and the vertically parallel walls are kept constant. As a result, no-slip criteria were given for the remaining two walls). These results are performed for Ha varies by 0,10,25 and 50, inclination angle θ varies by $0, \frac{\pi}{6}, \frac{\pi}{4}, \frac{\pi}{3}$ and $\frac{\pi}{2}$ and for fixed $Re = 1$. Here, we can observe how increasing the magnetic force has an impact on the flow and how the inclination angle θ for magnetic force affects the flow. Figure 5,6,7,8 and 9 displays streamline plots for various values of Ha (as 10, 25 and 50) for cases $\theta = 0, \frac{\pi}{6}, \frac{\pi}{4}, \frac{\pi}{3}$ and $\frac{\pi}{2}$ respectively.

Figure 5 presents the streamline plots which show the Stokes MHD fluid flow after reaching the steady state for increasing values of Ha from 10 to 50 and for fix $Re = 1$ and inclination angle $\theta = 0$ in square domain with top and bottom walls moving in the clockwise direction. In figures 5a, 5b and 5c, we observe that all the three streamline plots are symmetric to the line $x_2 = 0.5$ and there are two primary vortices formed in each case one is above to the line $x_2 = 0.5$ and another is below to the line $x_2 = 0.5$. One of the primary causes for the appearance of these vortices at these specific positions in the direction of moving lids. In figure 5a and 5b (cases

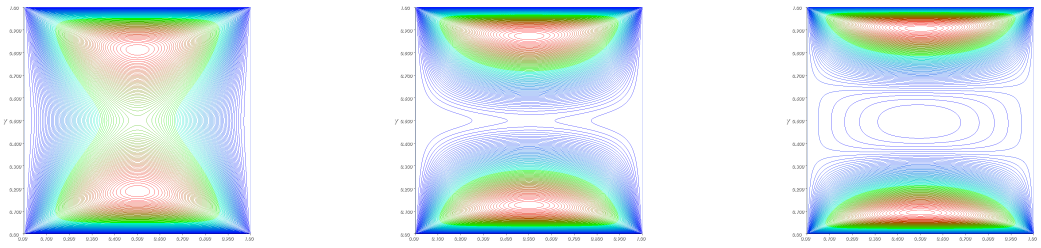

(A) Ha=10 (B) Ha=25 (C) Ha=50

FIGURE 5. Streamlines for Stokes MHD for $\theta = 0$

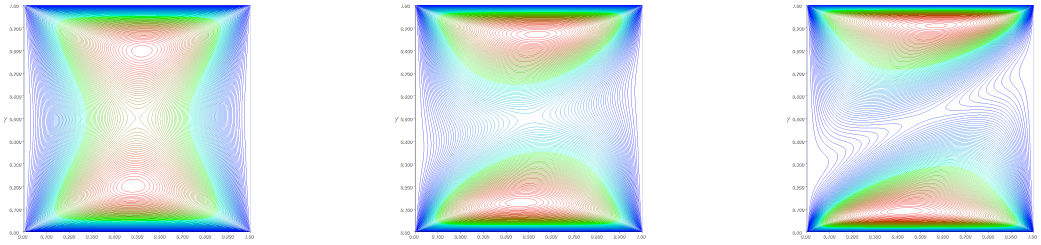

(A) Ha=10 (B) Ha=25 (C) Ha=50

FIGURE 6. Streamlines for Stokes MHD for $\theta = \frac{\pi}{6}$

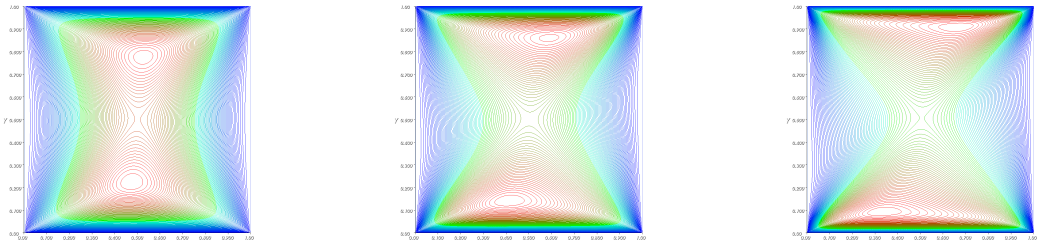

(A) Ha=10 (B) Ha=25 (C) Ha=50

FIGURE 7. Streamlines for Stokes MHD for $\theta = \frac{\pi}{4}$

of $Ha = 10$ and 25) secondary vortex has not appeared but in figure 5c secondary vortices are formed in the middle of the domain.

Figure 6 presents the streamlines plots for $Ha = 0, 25$ and 50 and inclination angle $\theta = \frac{\pi}{6}$ in a square cavity with top and bottom walls are moving in the clockwise direction. Figure 6 shows how the values of Ha and the inclination angle $\theta = \frac{\pi}{6}$ affect the formation of vortices. In figures 6a, 6b and 6c, we notice that there are two primary vortices formed in each case one is above the line $x_2 = 0.5$ and another is below to the line $x_2 = 0.5$ but here streamline plots are asymmetric to the line $x_2 = 0.5$. The major causes behind these vortices are the direction of moving lids and the inclination angle.

Figure 7 shows the streamlines plots for Stokes MHD in case of $Ha = 10, 25 \text{and} 50$ and inclination angle $\theta = \frac{\pi}{4}$ in square domain with top and bottom lids are moving

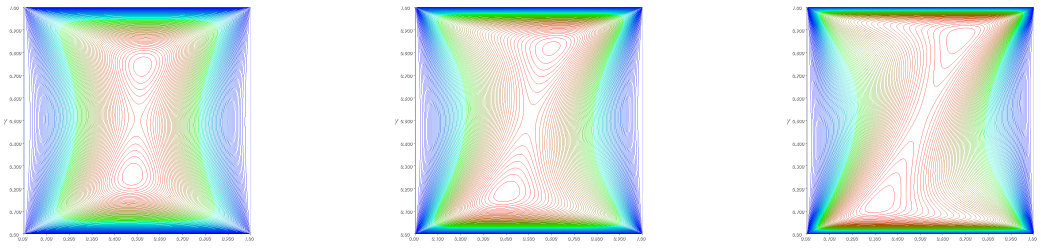

(A) Ha=10 (B) Ha=25 (C) Ha=50

FIGURE 8. Streamlines for Stokes MHD for $\theta = \frac{\pi}{3}$

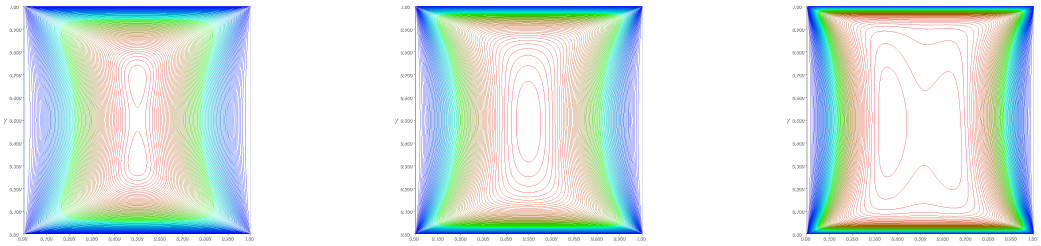

(A) Ha=10 (B) Ha=25 (C) Ha=50

FIGURE 9. Streamlines for Stokes MHD for $\theta = \frac{\pi}{2}$

in the clockwise direction. In figures 7a,7b and 7c, We see that two major vortices are generated in each case, one above the line $x_2 = 0.5$ and the other below it, asymmetrically. In figures of 7 streamlines show the effect of Ha values, the inclination angle $\theta = \frac{\pi}{4}$, and the direction of moving lids.

Figure 8 displays the streamlines plots for Stokes MHD in case of $Ha = 10, 25\text{and}50$ and inclination angle $\theta = \frac{\pi}{3}$ in a square domain with top and bottom lids are rotating in the clock-wise direction. In figures 8a,8b and 8c, we observed that there are two primary vortices in each case. In the figures of 8, we can see how increasing values of Ha affects the flow by streamlines. The inclination angle $\theta = \frac{\pi}{3}$ and the direction of moving lids also affect the flow along with Ha.

Figure 9 presents streamline plots for Stokes MHD in case of $Ha = 10, 25$ and 50 and inclination angle $\theta = \frac{\pi}{2}$ in square domain with top and bottom walls rotated in the clockwise direction. In figure 9a, we see that there are two primary vortices symmetric to the line $x_2 = 0.5$ whereas in figures 8b and 8c there is only one primary vortex and all the streamlines plots in figure 9 are symmetric about $x_2 = 0.5$. In the figures of 9, we can see how Ha values and the direction of moving walls affect the flow by streamlines.

Figures in 10 presents the horizontal velocity plots along $x_1 = 0.5$ for different inclination angles $\theta = 0, \frac{\pi}{6}, \frac{\pi}{4}, \frac{\pi}{3}$ and $\frac{\pi}{2}$ and fix the values of Ha. Similarly, figures in 11 show the vertical velocity plots along $x_2 = 0.5$ for the same cases mentioned for

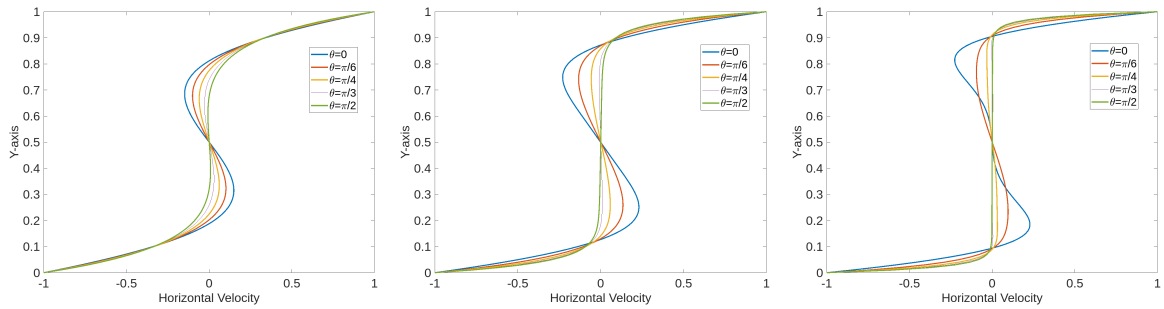

(A) Ha=10 (B) Ha=25 (C) Ha=50

FIGURE 10. Horizontal Velocity plots along $x_1 = 0.5$ with varying θ by $0, \frac{\pi}{6}, \frac{\pi}{4}, \frac{\pi}{3}$ and $\frac{\pi}{2}$

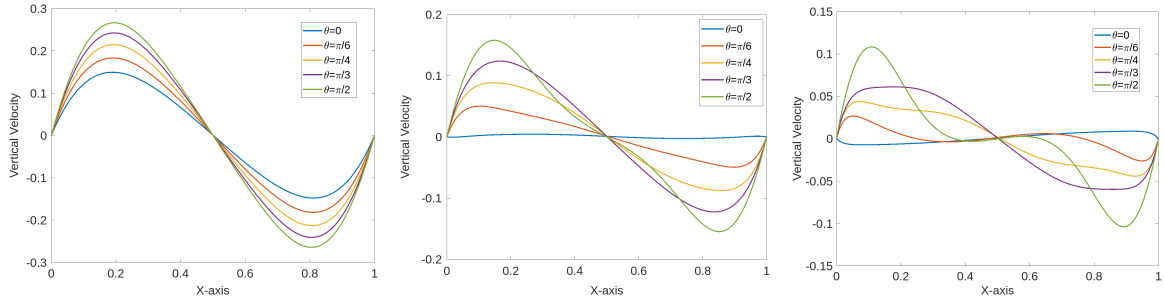

(A) Ha=10 (B) Ha=25 (C) Ha=50

FIGURE 11. Vertical Velocity plots along $x_2 = 0.5$ with varying θ by $0, \frac{\pi}{6}, \frac{\pi}{4}, \frac{\pi}{3}$ and $\frac{\pi}{2}$

horizontal velocity. Figures 10 and 11 show the variations in horizontal and vertical velocities from one boundary to the other among the pairs of parallel walls.

Figures 12 and 13 show horizontal and vertical velocities along the lines $x_1 = 0.5$ and $x_2 = 0.5$ respectively for different values of $Ha = 0, 10, 25$ and 50 and fix the values of θ. These figures show the variations in horizontal and vertical velocities by increasing the values of Ha for different inclination angles.

4. CONCLUSION

This article presents the results obtained for solving the transient Stokes MHD (Magnetohydrodynamic) problem for fixing Reynolds number $Re = 1$ different values of Hartmann number Ha ranging from 0 to 50 in square domain with their top and bottom parallel boundary lids moving horizontally to clock-wise direction. Since the MHD term in the governing equations depends on the inclination angle θ. Therefore, the numerical solution of Stokes MHD equation is described for different inclination angles $\theta = 0, \frac{\pi}{6}, \frac{\pi}{4}, \frac{\pi}{3}$ and $\frac{\pi}{2}$. Here, an in-depth discussion is provided on the key observations pertaining to the development of vortices and their varied patterns. In general, two major vortices formed for inclination angles $\theta = 0, \frac{\pi}{6}, \frac{\pi}{4}$ and $\frac{\pi}{3}$ in each

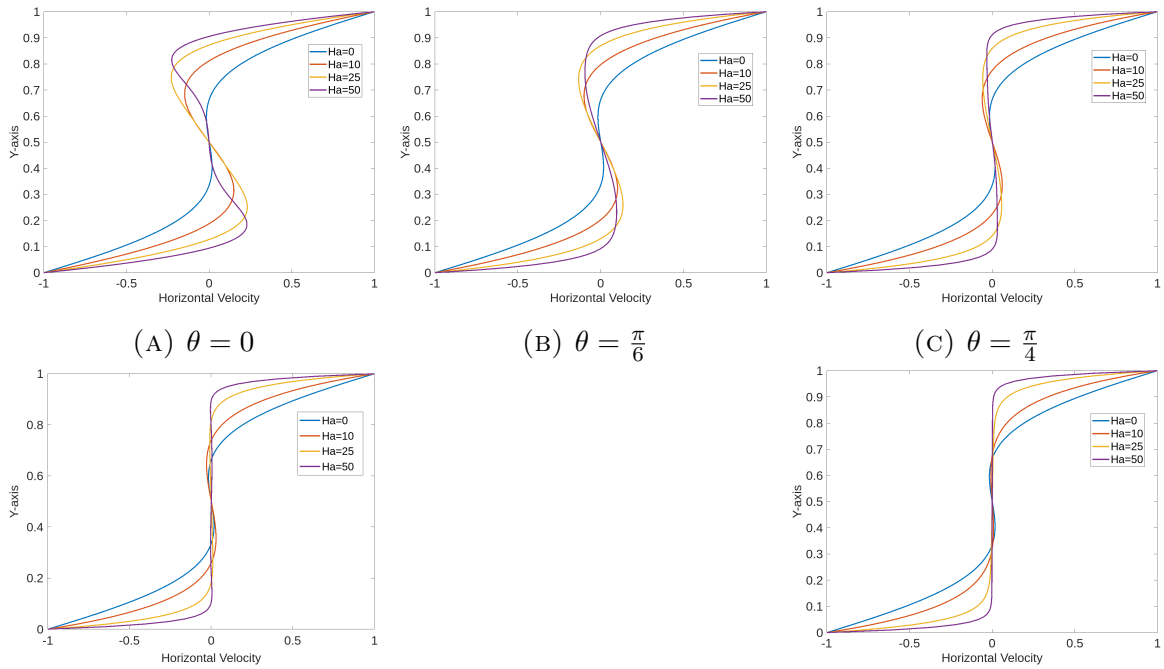

(A) $\theta = 0$ (B) $\theta = \frac{\pi}{6}$ (C) $\theta = \frac{\pi}{4}$

(D) $\theta = \frac{\pi}{3}$ (E) $\theta = \frac{\pi}{2}$

FIGURE 12. Horizontal Velocity plots along $x_1 = 0.5$ with varying Ha by 0,10,25 and 50

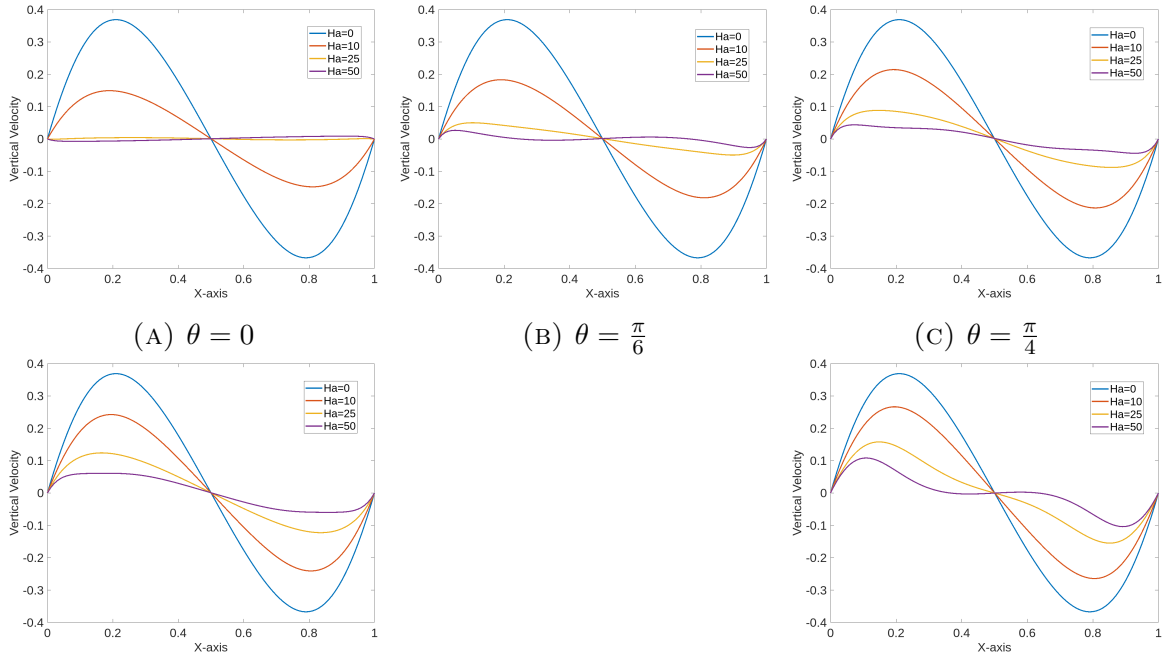

(A) $\theta = 0$ (B) $\theta = \frac{\pi}{6}$ (C) $\theta = \frac{\pi}{4}$

(D) $\theta = \frac{\pi}{3}$ (E) $\theta = \frac{\pi}{2}$

FIGURE 13. Vertical Velocity plots along $x_2 = 0.5$ with varying Ha by 0,10,25 and 50

case of Hartmann number ($Ha = 10, 25$ and 50). In the case of inclination angle $\theta = \frac{\pi}{2}$, two primary vortices only form in the case of Ha = 10 and only one vortex appears in the other cases of $Ha = 25$ and 50. The secondary vortex appears only for the case $Ha = 50$ and $\theta = 0$ in the middle of the square domain. The shapes and sizes of primary and secondary vortices are significantly influenced by the Hartmann numbers as well as the inclination angle. Along the horizontal and vertical mid-planes, the velocity solution plots are also displaying how they change from one boundary to the next among the parallel wall pairs. By adjusting the Hartmann number and inclination angle, we may observe the variation in horizontal and vertical velocities. This study contributes significantly to the Newtonian fluid flow problem by covering a wide range of significant aspects of the Stokes MHD fluid flow behavior in doubly driven cavity flow in the square domain.

REFERENCES

[1] N.G. Triantafillopoulos and C.K. Aidun, Relationship between flow instability in short-dwell ponds and cross directional coat weight nonuniformities, *Tappi journal*, 73:127–136, 1990.

[2] D.L. Stefanovic and H.G. Stefan, Simulation of transient cavity flows driven by buoyancy and shear, *Journal of Hydraulic Research*, 38:185–195, 2000.

[3] N. Alleborn, H. Raszillier, and F. Durst, Lid-driven cavity with heat and mass transport, *International Journal of Heat and Mass Transfer*, 42:833–853, 1999.

[4] P. Zdanski, M. Ortega, and N.G.F. Jr, Numerical study of the flow over shallow cavities, *Computers & fluids*, 32:953–974, 2003.

[5] C. Bruneau and M. Saad, The 2D lid-driven cavity problem revisited, *Computers & fluids*, 35:326–348, 2006.

[6] A. Cortes and J. Miller, Numerical experiments with the lid driven cavity flow problem, *Computers & fluids*, 23:1005–1027, 1994.

[7] E. Aslan, I. Taymaz, and A.C. Benim, Investigation of the lattice Boltzmann SRT and MRT stability for lid driven cavity flow, *International Journal of Materials, Mechanics and Manufacturing*, 2:317–324, 2014.

[8] T.A. AbdelMigid, K.M. Saqr, M.A. Kotb, and A.A. Aboelfarag, Revisiting the lid-driven cavity flow problem: Review and new steady state benchmarking results using GPU accelerated code, *Alexandria Engineering Journal*, 56:123–135, 2017.

[9] A.M. Grillet, B. Yang, B. Khomami, and E.S.G. Shaqfeh, Modeling of viscoelastic lid driven cavity flow using finite element simulations, *Journal of Non-Newtonian Fluid Mechanics*, 88:99–131, 1999.

[10] S. Haque, I. Lashgari, F. Giannetti, and L. Brandt, Stability of fluids with shear-dependent viscosity in the lid-driven cavity, *Journal of Non-Newtonian Fluid Mechanics*, 173:49–61, 2012.

[11] A. Syrakos, G. Georgiou, and A. Alexandrou, Solution of the square lid-driven cavity flow of a Bingham plastic using the finite volume method, *Journal of Non-Newtonian Fluid Mechanics*, 195:19–31, 2013.

[12] U. Ghia, K.N. Ghia, and C.T. Shin, High-Re Solutions for Incompressible Flow Using the Navier-Stokes Equations and a Multigrid Method, *Journal of computational physics*, 48:387–411, 1982.

[13] H. Kuhlmann, M. Wanschura, and H. Rath, Flow in two-sided lid-driven cavities: non-uniqueness, instabilities, and cellular structures, *Journal of Fluid Mechanics*, 336:267–299, 1997.

[14] S. Albensoeder, H. Kuhlmann, and H. Rath, Multiplicity of steady two-dimensional flows in two-sided lid-driven cavities, *Theoretical and Computational Fluid Dynamics*, 14:223–241, 2001.

[15] C. Blohm and H. Kuhlmann, The two-sided lid-driven cavity: experiments on stationary and time-dependent flows, *Journal of Fluid Mechanics*, 450:67–95, 2002.

[16] D.A. Perumal and A. Dass, Simulation of flow in two-sided lid-driven square cavities by the lattice Boltzmann method, *WIT Transactions on Engineering Sciences*, 59:45–54, 2008.

[17] D.A. Perumal and A. Dass, Simulation of Incompressible Flows in Two-Sided Lid-Driven Square Cavities.: Part I-FDM, *CFD Letters*, 2:13–24, 2010.

[18] D.A. Perumal and A. Dass, Multiplicity of steady solutions in two-dimensional lid-driven cavity flows by lattice Boltzmann method, *Computers & Mathematics with Applications*, 61:3711–3721, 2011.

[19] K.-T. Chen, C.-C. Tsai, W.-J. Luo, and C.-N. Chen, Aspect Ratio Effect on Multiple Flow Solutions in a Two-Sided Parallel Motion Lid-Driven Cavity, *Cambridge University Press*, 31:153–160, 2014.

[20] S. Arun and A. Satheesh, Analysis of flow behaviour in a two sided lid driven cavity using lattice Boltzmann technique, *Alexandria Engineering Journal*, 54:795–806, 2015.

[21] J.M. Cadou, Y. Guevel, and G. Girault, Numerical tools for the stability analysis of 2D flows: application to the two-and four-sided lid-driven cavity, *Fluid Dynamics Research*, 44:1–12, 2012.

[22] F. Hammami, B. Souayeh, N. Ben-Cheikh, and B. Ben-Beya, Computational analysis of fluid flow due to a two-sided lid driven cavity with a circular cylinder, *Computers & Fluids*, 156:317–328, 2017.

[23] O.A. Bég, S.K. Ghosh, T.A. Bég, Applied magnetofluid dynamics: modelling and computation, *LAP LAMBERT ACADEMIC PUBL* 445, 2011.

[24] C. Qi, C. Wu, Electromagnetohydrodynamic flow in a rectangular microchannel, *Sensors and Actuators B: Chemical*, 263:643–660, 2018.

[25] D.J. Laser and J.G. Santiago, A review of micropumps, *Journal of micromechanics and microengineering*, 14:R35–R64, 2004.

[26] C. Das, G. Wang and F. Payne, Some practical applications of magnetohydrodynamic pumping, *Sensors and Actuators A: Physical*, 201:43–48, 2013.

[27] S. Ganesh and S. Krishnambal, Unsteady Magnetohydrodynamic stokes flow of viscous fluid between two parallel porous plates, *Journal of Applied Sciences*, 7:374–379, 2007.

[28] R.M. Terril, G.M. Shrestha, Laminar flow through channels with porous walls and with an applied transverse magnetic field, *Applied Scientific Research, Section B*, 11:134–144, 1964.

[29] M. Pirmohammadi and M. Ghassemi, Effect of magnetic field on convection heat transfer inside a tilted square enclosure, *International Communications in Heat and Mass Transfer*, 36:776–780, 2009.

[30] F.S. Oğlakkaya and C. Bozkaya, Unsteady MHD mixed convection flow in a lid-driven cavity with a heated wavy wall, *International Journal of Mechanical Sciences*, 148:231–245, 2018.

[31] M. Gürbüz and M. Tezer-Sezgin, MHD Stokes flow in lid-driven cavity and backward-facing step channel, *European Journal of Computational Mechanics*, 24:279–301, 2015.

[32] F. Brezzi, On the existence, uniqueness and approximation of saddle-point problems arising from Lagrangian multipliers, *Publications des séminaires de mathématiques et informatique de Rennes*, S4:1–26, 1974.

[33] V. Girault and P.A. Raviart, Finite Element Approximation of the Navier-Stokes Equations, *Lecture Notes in Math.,* 749, 1979.

[34] R. Stenberg, Analysis of Mixed Finite Element Methods for the Stokes Problem: A Unified Approach, *Mathematics of Computation*, 42:9–23, 1984.

[35] D. Boffi, F. Brezzi and M. Fortin, Mixed Finite Elements and Applications, *Springer*, 44, 2013.